

Faculty of Engineering

Faculty of Engineering - Papers

University of Wollongong

Year 2002

Intrinsic nanostructural domains:
Possible origin of weaklinkless
superconductivity in the quenched
reaction product of Mg and amorphous B

S. Li* O. Prabhakar[†] T. T. Tan[‡]
C. Q. Sun** X. L. Wang^{††} S. Soltanian^{‡‡}
 J. Horvat[§] S. X. Dou[¶]

*Nanyang Technological University, Singapore

[†]Nanyang Technological University, Singapore

[‡]Nanyang Technological University, Singapore

**Nanyang Technological University, Singapore

^{††}University of Wollongong, xiaolin@uow.edu.au

^{‡‡}University of Wollongong, saeid@uow.edu.au

[§]University of Wollongong, jhorvat@uow.edu.au

[¶]University of Wollongong, shi@uow.edu.au

This article was originally published as: Li, S, Prabhakar, O, Tan, TT, Sun, CQ, Wang, XL, Soltanian, S, Horvat, J & Dou, SX, Intrinsic nanostructural domains: Possible origin of weaklinkless superconductivity in the quenched reaction product of Mg and amorphous B, Applied Physics Letters, 2002, 81(5), 874-876, and may be found here. Copyright 2002 American Institute of Physics. This article may be downloaded for personal use only. Any other use requires prior permission of the author and the American Institute of Physics.

This paper is posted at Research Online.

<http://ro.uow.edu.au/engpapers/94>

Intrinsic nanostructural domains: Possible origin of weaklinkless superconductivity in the quenched reaction product of Mg and amorphous B

S. Li,^{a)} O. Prabhakar, T. T. Tan, and C. Q. Sun

School of Materials Engineering, Nanyang Technological University, Singapore 639798

X. L. Wang, S. Soltanian, J. Horvat, and S. X. Dou

Institute of Superconducting and Electronic Materials, University of Wollongong, NSW 2522, Australia

(Received 9 April 2002; accepted for publication 3 June 2002)

Smooth modulation structure of Mg–B alloy in the quenched reaction product of Mg and amorphous B was studied. It indicates that the MgB₂ formed possibly in spinodal decomposition, thus resulting in MgB₂ nanodomains. It was found that the nanodomains with small angle boundaries of atomic-scale width were distributed within the subgrains that constitute the clusters in MgB₂ grains. This nanostructural characteristic may be intrinsic in the quenched reaction product of Mg and amorphous B. It makes the nanodomain boundaries not act as barriers to the current percolation path, thus exhibiting no weak-link problem in the MgB₂. © 2002 American Institute of Physics. [DOI: 10.1063/1.1497712]

The discovery of superconductivity at 39 K in MgB₂ has initiated enormous scientific interest to understand and develop this material because of its high performance for magnetic and electronic applications.^{1,2} The strongly linked current flow measured from polycrystalline MgB₂ shows that this new superconductor class is not compromised by a weak-link problem.³ The experimental results have demonstrated that high critical current density (J_c) can be achieved in a dense MgB₂ wire, which was prepared by exposing crystalline boron filaments to Mg vapor.⁴ The achievement of 85 000 A/cm² at 4.2 K in a high dense Fe-clad MgB₂ tape fabricated with powder-in-tube (PIT) technique also promised the potential large-scale applications of this material.⁵ However, MgB₂ thin films still exhibit higher J_c (Ref. 6) comparing with bulk materials. It is not clear whether this phenomenon is due to anisotropic superconducting properties of the MgB₂ although anisotropic superconducting properties do exist in single crystal, in thin films as well as in the aligned crystals.^{6–9} For the high-field performance of MgB₂, it was reported that a lack of natural defects might be responsible for the rapid decline of J_c with increasing field strength.¹⁰ Proton irradiation, therefore, was used to displace atoms from their equilibrium lattice sites, creating a variety of defects to depress the superconducting order parameters locally, and thereby create pinning sites to enhance the high-field J_c in MgB₂.¹¹ It is also believed that extremely small grains would be consistent with strong grain boundary pinning.¹² Moreover, air quenching the reaction product of Mg and amorphous B is a common technique to obtain MgB₂ superconducting material employed by a number of research groups. Although the structural feature of MgB₂ was preliminarily investigated with high-resolution transmission electron microscopy (HRTEM),¹³ the origin of the weaklinkless superconductivity and also the nanostructural

characteristics of the material are still not clear. In this letter, we report the observation of MgB₂ nanodomains in the quenched reaction product of Mg and amorphous B and the origin of weaklinkless superconductivity in this material.

The Fe-clad MgB₂ wire was prepared by PIT technique using a mixture of magnesium 99% purity and amorphous boron 99% purity powders in the stoichiometric ratio of Mg:B=1:2. The composite tube was drawn into ϕ 1 mm wires from ϕ 10 mm by multistep drawing. In order to investigate the nanostructural characteristics of MgB₂, short samples in lengths of 2 cm were sealed in a small Fe tube and annealed at 745 °C–840 °C for 5–60 min in pure Ar atmosphere and then quenched in air. X-ray diffraction (XRD) showed that the high purity of MgB₂ (above 90%) was obtained by using the aforementioned techniques.¹⁴ Subsequently the treated wire was mounted into a copper tube of ϕ 3 mm with epoxy and then was sliced, dimpled, and ion-beam milled to prepare the samples for HRTEM characterization.

Figure 1(a) shows a grain (\sim 200 nm) consisting of a cluster MgB₂ subgrains. The size of the subgrains is only one twentieth (\sim 10 nm) of the grain size. This phenomenon pre-

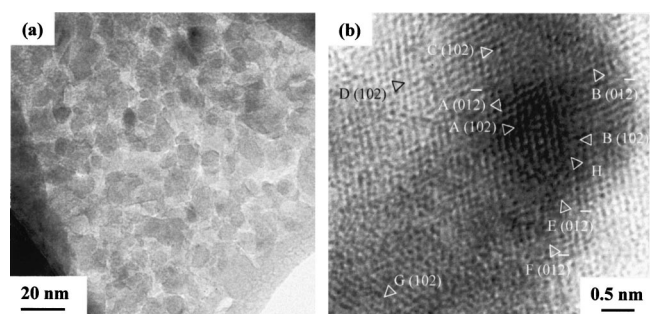


FIG. 1. (a) HRTEM micrograph showing that the MgB₂ grains consisted of a cluster of subgrains and the grain boundary of the adjacent MgB₂ grains was constructed by the boundaries of subgrains. (b) HRTEM micrograph reveals the nanostructural characteristics of the MgB₂, which a nanodot was surrounded by nanodomains with small angle boundaries.

^{a)}Author to whom correspondence should be addressed; electronic mail: assxli@ntu.edu.sg

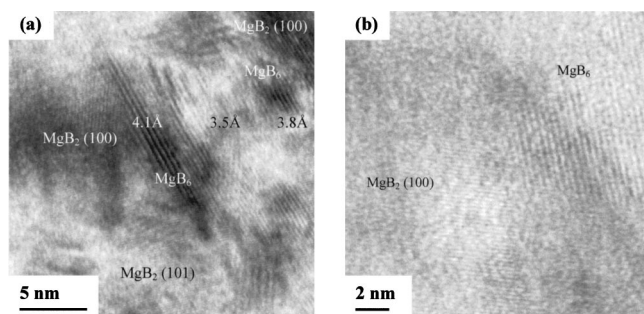


FIG. 2. (a) HRTEM micrograph exhibits smooth variations of lattice fringes with a range of 8.5 nm and a number of MgB_2 lattice fringes are discernible. (b) MgB_2 formed beside the nonequilibrium MgB_6 observed in the other area.

dominated the microstructure of the materials. HRTEM image in Fig. 1(b) exhibits a two-dimensional lattice image of a $1 \times 1 \text{ nm}^2$ MgB_2 nanodot (marked with A), which was surrounded by a few nanodomains with small angle boundaries. It can be clearly seen that the angle of the boundaries between $(01\bar{2})$ of nanodot A and $(01\bar{2})$ of nanodomain B was 3° , and the angle of the boundaries between (102) of nanodot A and (102) of nanodomain C was 7° , respectively. Other small angles, such as 5° between A (102) and B (102) , 5° between C (102) and D (102) , 5° between E $(01\bar{2})$ and F $(01\bar{2})$, and also 10° between A $(01\bar{2})$ and E $(01\bar{2})$, were observed in Fig. 1. However, the (102) plane of a nanodomain (marked with G), that was apart from the nanodot, having a large angle of 45° misorientation with the (102) plane of nanodot A is discernible. This indicates that the subgrain actually consisted of a cluster of MgB_2 nanodomains (1–4 nm) and the majority of the nanodomains distributed in the subgrain with small angle boundaries. Moreover, the right- and left-hand side edge (102) planes of nanodomains A and B joined together at point H. It can be inferred that the space between these two planes is the boundary of the nanodomains and the width of the boundary is in atomic scale, which is much smaller than the coherent length of MgB_2 that is 50 \AA .^{4,5}

Smooth variations of atomic plane spaces (d spacings) from 4.1 to 3.5 \AA and then to 3.8 \AA in a span of 8.5 nm were observed in the samples [Fig. 2(a)]. 4.1 and 3.8 \AA correspond to the d spacings of MgB_6 which are 4.19 and 3.79 \AA while 3.5 \AA is close to the d spacing of MgB_2 (001) which is 3.52 \AA . No d spacing in other possible compounds and elements, such as MgB_4 , MgB_7 , MgB_{12} , MgO , Mg , and B is around 4.1 \AA within the measurement error. Therefore, the correlated lattice fringe can be identified as belonging to MgB_6 . It is rather difficult to index the planes for MgB_6 because the information on its lattice parameters and structure system are not available in Powder Diffraction File (08-0421) although a number of d spacing data have been listed. However, it is clear that the observed smooth variation of the d spacings was attributed to the variations in lattice parameters caused by the composition modulations of B in the crystal and the d spacing decreased/increased with the abundance of B decreasing/increasing in the crystal. A lattice fringe of MgB_2 (100) formed on top of MgB_6 is discernible and a similar phenomenon can also be found in other regions of the sample analyzed [Fig. 2(b)]. It seems the B-less nanodomain,

MgB_2 , always formed beside the B-rich nanodomain, MgB_6 . This phenomenon combining with the modulation d spacing of a Mg–B alloy implies that the MgB_2 nanodomains usually form by the spinodal decomposition. For spinodal decomposition to occur, the initial and final structures should share a common lattice or lack of lattice, as in liquids and glasses.¹⁵ In addition, the phase diagram should indicate miscibility gap. It is not very easy to experimentally follow the spinodal decomposition. However, HRTEM lattice images technique has been employed and a smooth variation of spacing of adjacent lattice planes undergoing phase separation¹⁶ has been attributed to variations in lattice parameter caused by composition modulations as in spinodal decomposition. In the structure studied, the percentage of B varies from 66.67% to 85.5% as the structure varied from MgB_2 to MgB_6 suggesting the formation of many metastable reactions by continuous mechanism. This suggests the possibility of spinodal decomposition.

It is believed that MgB_2 forms via a process of diffusion of Mg vapor into boron,⁴ producing a supersaturated Mg–B solution. The composition fluctuations caused by the random arrangement of B atoms in the amorphous phase caused variations of the coordination numbers around Mg atoms, thus resulting in the modulation structure in the supersaturated solution. However, the amplitude of the composition modulations should not have too much deviation from the chemical stoichiometry of MgB_2 . Therefore, by deeply quenching the materials into the miscibility gaps of Mg– MgB_2 and MgB_2 – MgB_4 , the majority of the reaction products (>90%) are MgB_2 based on the application of lever rule to the phase diagram. This has been proved by XRD analysis.¹⁴ Although MgB_6 is a nonequilibrium phase unlike the equilibrium phases of MgB_4 and MgB_7 in Mg–B binary phase diagram, it was often observed by HRTEM. It is believed that the reaction path of the Mg–B supersaturated solution is rather complex, sometimes involving the formation of one or more intermediate nonequilibrium phases, such as MgB_6 , prior to reaching the equilibrium two-phase microstructures.^{16,17} The observation of the nonequilibrium MgB_6 formation was also reported by other research groups^{7,13} even though MgB_4 was detected more frequently in the experiments. However, the determination of the multiphase nature in the samples is difficult due to the sensitivity of XRD to such a small fraction of the other phases.

Figure 3 exhibits field dependence of J_c calculated from M – H loops using the Bean critical theory in the samples treated with various processing parameters, such as different annealing temperatures and durations, but all the samples were quenched in air. Obviously, if MgB_2 was formed by a nucleation and growth mechanism, the various thermal treatment parameters would result in different microstructures, such as grain size, etc., thus strongly affecting the field dependence of J_c .⁹ However, the samples treated with different thermal parameters had similar J_c at a particular measurement temperature, such as 10, 15, 20, and 30 K, respectively, as shown by groups of dotted, dashed, and solid lines in Fig. 3. This implies that J_c is independent of the thermal treatment parameters and it may be dominated by the spinodal decomposition microstructure formed in the quench processing. The relative lower J_c in this study may be due to the fact

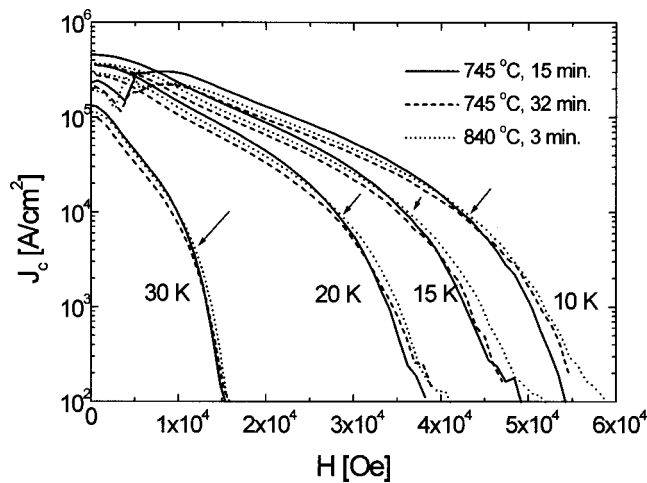


FIG. 3. Field dependence of J_c measured from the samples treated with various processing parameters, such as annealing temperature and duration.

that the fabrication parameters were not optimized. Although the quenched MgB_2 produced by the Mg vapor and crystalline B also shows a higher J_c of $3 \times 10^5 \text{ A/cm}^2$ and 400 A/cm^2 at 5 K in 0 and 6 T, respectively,⁴ further study is needed to clarify whether the spinodal decomposition only occurred in quenching the reaction product of Mg and amorphous B. The composition fluctuation in amorphous B may be the intrinsic origin to cause the spinodal decomposition in the quenched MgB_2 , resulting in the formation of MgB_2 nanodomains.

A magneto-optical image of an air quenched MgB_2 slab demonstrates that almost no spatial variation of J_c is visible.^{2,18} This suggests that there is no inherent string suppression of current across the grain boundaries. Obviously, the current percolation behavior in the quenched MgB_2 is determined by the nanodomains that constituted the subgrains in the clusters. In this case, the boundaries of nanodomains play an important role to affect the J_c instead of the grain boundaries, which were actually the boundaries of subgrains. Since the width of the small angle boundaries between the adjacent nanodomains is much smaller than the coherent length of MgB_2 , the boundaries may not act as weak-link barriers to the current percolation paths. This may be why the MgB_2 does not show that “weak-link” effect characteristic of the high- T_c superconductors. In fact, the large grains of $200 \mu\text{m}$ in the sample sintered at $800 \text{ }^\circ\text{C}$ for 4 h following furnace cooling decouple at high field,¹⁹ while the nanodomain boundaries in the samples sintered at $745 \text{ }^\circ\text{C}$ – $840 \text{ }^\circ\text{C}$ for 5–30 min subsequently air quenched present no barrier to the current.¹⁴ This shows that the nanodomain boundaries are transparent to the percolated current.

In summary, the observation of the modulation lattice d spacing of a Mg–B alloy reveals that the MgB_2 forms in the spinodal decomposition, which results the MgB_2 nanodomains in the subgrains of the clusters. The nanodomains may be the intrinsic structure in the quenching reaction product of Mg and amorphous B and the boundaries of the nanodomains are in the atomic scale that is much smaller than the coherent length of MgB_2 . The nanodomains distribute in the subgrains with small angle boundaries. It is believed that this nanostructural characteristic is the origin to overcome the weak-link problem of high- T_c superconducting oxides.

- ¹J. Nagamatsu, N. Nakagawa, T. Muranaka, Y. Zenitani, and J. Akimitsu, *Nature* (London) **410**, 63 (2001).
- ²D. Larbalestier, A. Gurevich, D. M. Feldmann, and A. Polyanskii, *Nature* (London) **414**, 368 (2001).
- ³D. C. Larbalestier, L. D. Cooley, M. O. Rikel, A. A. Polyanski, J. Jiang, S. Patnalk, X. Y. Cai, D. M. Feldmann, A. Gurevich, A. A. Squitieri, M. T. Naus, C. B. Eom, E. E. Hellstrom, R. J. Cava, K. A. Regan, N. Rogado, M. A. Hayward, T. He, J. S. Slusky, K. Khalifah, K. Inumaru, and M. Haas, *Nature* (London) **410**, 186 (2001).
- ⁴P. C. Canfield, D. K. Finnemore, S. L. Bud'ko, J. E. Ostenson, G. Lapertot, C. E. Cunningham, and C. Petrovic, *Phys. Rev. Lett.* **86**, 2423 (2001).
- ⁵S. Jin, H. Mavoori, C. Bower, and R. B. van Dover, *Nature* (London) **411**, 563 (2001).
- ⁶W. N. Kang, H. J. Kim, E. M. Choi, C. U. Jung, and S. I. Lee, *Science* **292**, 1521 (2001).
- ⁷S. Lee, H. Mori, T. Masui, Y. Eltsev, A. Yamamoto, and S. Tajima, *J. Phys. Soc. Jpn.* **70**, 2255 (2001).
- ⁸O. F. de Lima, R. A. Ribeiro, M. A. Avila, C. A. Cardoso, and A. A. Coelho, *Phys. Rev. Lett.* **86**, 5974 (2001).
- ⁹A. K. Pradhan, Z. X. Shi, M. Tokunage, T. Tamegai, Y. Takano, K. Togano, H. Kito, and H. Ihara, *Phys. Rev. B* **64**, 212509 (2001).
- ¹⁰Y. Bugoslavsky, G. K. Perkins, X. Qi, L. F. Cohen, and A. D. Caplin, *Nature* (London) **410**, 563 (2001).
- ¹¹Y. Bugoslavsky, L. F. Cohen, G. K. Perkins, M. Pollchetti, T. J. Tate, R. Gwilliam, and A. D. Caplin, *Nature* (London) **411**, 561 (2001).
- ¹²C. B. Eom, M. K. Lee, J. H. Chol, L. J. Belenky, X. Song, L. D. Cooley, M. T. Naus, S. Patanik, J. Jiang, M. Rikei, A. Polyanski, A. Gurevich, X. Y. Cai, S. D. Bu, S. E. Babcock, E. E. Hellstrom, D. C. Larbalestier, N. Rogado, K. A. Regan, M. A. Hayward, T. He, J. S. Slusky, K. Inumaru, M. K. Haas, and R. J. Cava, *Nature* (London) **411**, 558 (2001).
- ¹³J. Q. Li, L. Li, Y. Q. Zhou, Z. A. Ren, G. C. Che, and Z. X. Zhao, *cond-mat/0104350*.
- ¹⁴X. L. Wang, S. Soltanian, J. Horvat, A. H. Liu, M. J. Qin, H. K. Liu, and S. X. Dou, *Physica C* **361**, 149 (2001).
- ¹⁵R. D. Doherty, *Physical Metallurgy Part II*, 3rd edition, edited by R. W. Cahn and P. Haasen (Elsevier Science, New York, 1983), p. 933.
- ¹⁶R. Wagner, R. Kampmann, and P. W. Voorhees, *Phase Transformation in Materials*, edited by G. Kostorz (Wiley-VCH, Weinheim, 2001), p. 309.
- ¹⁷T. B. Massalski, H. Okamoto, P. R. Subramanian, and L. Kacprzak, *Binary Alloy Phase Diagrams* (ASM International, Materials Park, Ohio, 1990), p. 498.
- ¹⁸A. A. Polyanskii, A. Gurevich, J. Jang, D. C. Larbalestier, S. L. Bud'ko, D. K. Finnemore, G. Lapertot, and P. C. Canfield, *Supercond. Sci. Technol.* **14**, 811 (2001).
- ¹⁹S. X. Dou, X. L. Wang, J. Horvat, D. Milliken, A. H. Li, K. Konstantinov, E. W. Collings, M. D. Sumption, and H. K. Liu, *Physica C* **361**, 79 (2001).